Iraqi Journal of Physics, 2026
https://doi.org/10.30723/ijp.v24i1.1381

Vol.24, No.1, PP. 12-20
P-ISSN: 2070-4003
E-ISSN: 2664-5548

Inelastic Electron Scattering (M2) for Changing Parity States of ^{12}C, ^{15}N and ^{24}Mg

Ali K. Abood[1*] and Ali A. Alzubadi[1]
[1]*Department of Physics, College of Science, University of Baghdad, Baghdad, Iraq*
[*]Corresponding author: ali.khaled1104a@sc.uobaghdad.edu.iq

Abstract
This study investigates the nuclear structure of ^{12}C, ^{15}N, and ^{24}Mg nuclei utilizing a shell model (SM) with the Skyrmee Hartree–Fock (SHF) approach. The form factors for inelastic electron scattering were computed for low-lying states that change their parity. This study demonstrates the practicality of the strategy using the truncated large-scale *spsdpf* shell model space with WBP two-body effective interaction. The data for the M2 transition (2^-,0),(2^-,1) states indicate energy levels of 12.180 MeV and 16.660 MeV in ^{12}C, 12.666 MeV in ^{24}Mg, 10.062 MeV and 10.800 MeV for $3/2^+_{(3)}$ and $3/2^+_{(4)}$ states, and 7.153 MeV and 10.529 MeV for $5/2^+_{(2)}$ and $5/2^+_{(4)}$ states in ^{15}N. Within Hartree-Fock theory, Skyrme interactions are utilized to derive a one-body potential for the computation of single-particle matrix elements. The single-particle potential of harmonic oscillator (HO), Woods-Saxon (WS), and SHF potentials for inelastic form factors exhibits a remarkable concurrence with the existing experimental data.

Article Info.

Keywords:
Shell Modell, Skyrmee Hartree-Fock, Changing Parity State, Inelastic Electron Scattering, Transverse Form Factor.

Article history:
Received: Oct. 11, 2024
Revised: Dec. 03, 2024
Accepted: Dec. 05, 2024
Published: Mar.01, 2026

1. Introduction
The two main approaches often used in nuclear structure research are the Shell Model (SM) and Self-Consistent Mean-Field (SCMF). Although they are both microscopic in scale, the two methods are complementary in their use of effective interactions, which makes them applicable to either very tiny places or various many-body wave functions [1]. Various nuclear chart elements, including anomalous nuclei, may have their decay and spectroscopy elucidated by empirical interactions in Subatomic Mechanics methods. While mean-field methods utilise a single global Hamiltonian to span the whole nuclear chart, the SM avoids this. In addition, the nuclear chart shows that the SCMF assigns different values to the binding energy, nuclear size, form factors, and surface deformation parameters, which are the fundamental nuclear attributes of the ground state. Two functions, which basically relate to the distribution of electric and magnetic charge within the nucleus, may be used to analyse the structure: the electric and magnetic form factors. Inelastic electron scattering in the nucleus involves directing high-energy electrons at atomic nuclei to study their internal structure and excitations. As a result, electron scattering plays a critical role in determining the effective dimensions of the nucleus and its charge distribution [2]. Configuration Mixing (CM) that exceeds the Mean Field (MF) is facilitated by the SM [3]. A traditional phenomenological single-particle model for the mean field may be used, using a configuration mixing computation that encompasses all many-body states derivable from a broad spectrum of single nucleon states around the Fermi energy[4].

This investigation uses the SM and HF methods to compute the inelastic electron scattering form factors for various parity states in the nucleus of ^{24}Mg, ^{12}C, and ^{15}N. Kanada-En'yo and Ogata [5] examined the negative-parity regimes of ^{24}Mg utilising proton and α inelastic scattering. The nuclear structure of the ^{24}Mg nucleus was investigated by Manie and Alzubadi [6] using the shell model and self-consistent Hartree-Fock computations. Form factors and transition probabilities for elastic and

inelastic electron scattering in both positive and negative low-lying states have been determined. Within the electron energy range of 90 to 280 MeV, Zarek et al. [7] computed the electromagnetic form factors for the main transitions to negative parity states in ^{24}Mg. Using inelastic electron scattering at backward scattering angles, Hicks et al. [8] measured magnetic excitations in ^{12}C with momentum transfers ranging from q = 0.5 to 3.3 fm^{-1}. Using a shortened Large-Scale Shell Model (LSSM) along with the Hartree–Fock technique, Alzubadi and Abbas [9] investigated the nuclear structure of particular isotopes $^{28, 29, 30}$Si. For positive and negative low-lying states, form factors, energy levels, and decreased transition probabilities have been assessed within the context of elastic and inelastic electron scattering. Alzubadi et al. [10] studied the elastic and inelastic electron scattering form factors for ^{25}Mg nucleus utilizing the SM with Hartree-Fock (HF) calculations. Al-Sammarraie et al.[11] calculated the total squared form factors, energy levels, and transition probability using the (PSDPF)Hamiltonian in a large model space (0 + 1) $\hbar\omega$. discussed the negative- parity states of ^{24}Mg nucleus within the shell model. Their study employed microscopic structure and reaction calculations involving both proton and α-particle probes. Sarriguren et al.[12] studied magnetic form factors from odd-A spherical and deformed nuclei corresponding to elastic electron scattering in the plane-wave Born approximation(PWBA).

The present study investigates nuclear excited states of differing parities in ^{24}Mg, ^{12}C, and ^{15}N within the framework of the SM, employing the Skyrme Hartree-Fock (SHF) method to generate the single-particle potential. The primary objective is to compute inelastic electro-excitation form factors using the valence model. Radial wave functions for the single-particle matrix elements corresponding to all excited states will be calculated using harmonic oscillator (HO), Woods-Saxon (WS), and SHF potentials.

2. Theoretical Formalism

The multipolarity electron scattering operator between the initial (*i*) and final (*f*) nuclear states is represented by the sum of products of the single-particle matrix elements multiplied by the one-body density matrix (OBDM), which constitutes the reduced nuclear matrix components [13]:

$$\left\langle f \left\| \hat{O}^{\lambda}(t_z) \right\| i \right\rangle = \sum_{ab} OBDM(f,i,a,b,\lambda,t_z) \left\langle a \left\| \hat{O}^{\lambda}(t_z) \right\| b \right\rangle \tag{1}$$

Let a and b represent the single-particle states (nlj) labels as a shorthand notation for the initial and final, with t_z equal to 1/2 for a proton and t_z equal to −1/2 for a neutron. The two-body interaction known as the Skyrme potential is used to calculate the central potential. It might be used to provide a one-body potential in Hartree-Fock theory, similar to codes that are now in use. To do this, the interaction dynamics between nucleons must first be modelled and then generate the magnetic field that each nucleon in the nucleus produces. The potential allows us to express V_{Skyrme} as [14]:

$$\begin{aligned}
&V_{Skyrme}(\vec{r}_1,\vec{r}_2) = t_0(1+x_0\hat{p}_\sigma)\delta_{12} + \frac{t_1}{2}(1+x_1\hat{p}_\sigma)\left[\vec{k}'^2\delta_{12} + \vec{k}^2\delta_{12}\right] \\
&+t_2(1+x_2\hat{p}_\sigma)k'\delta_{12}k + \frac{t_3}{6}(1+x_3\hat{p}_\sigma)p^\alpha\left(\frac{\vec{r}_1-\vec{r}_2}{2}\right)\delta_{12} + iW_0\vec{k}'\delta_{12}(\hat{\vec{\sigma}}_1+\hat{\vec{\sigma}}_2)\times\vec{k} \\
&+\frac{t_e}{2}\left(\left[3(\hat{\vec{\sigma}}_1.\vec{k}')(\hat{\vec{\sigma}}_2.\vec{k}') - (\hat{\vec{\sigma}}_1.\hat{\vec{\sigma}}_2)\vec{k}'^2\right] + \delta_{12}\left[3(\hat{\vec{\sigma}}_1.\vec{k})(\hat{\vec{\sigma}}_2.\vec{k}) - (\hat{\vec{\sigma}}_1.\hat{\vec{\sigma}}_2)\vec{k}^2\right]\right) \\
&+t_0\left[3(\hat{\vec{\sigma}}_1.\vec{k})\delta_{12}(\hat{\vec{\sigma}}_2.\vec{k}') - (\hat{\vec{\sigma}}_1.\hat{\vec{\sigma}}_2)\vec{k}'\delta_{12}\vec{k}'\right]
\end{aligned} \tag{2}$$

where

$$\delta_{12} = \delta(\vec{r}_1 - \vec{r}_2) \quad \textbf{(3)}$$

and

$$\hat{K} = \frac{1}{2i}(\vec{\nabla}_1 - \vec{\nabla}_2), \hat{K} = -\frac{1}{2i}(\vec{\nabla}'_1 - \vec{\nabla}'_2) \quad \textbf{(4)}$$

They operate on the wave functions to the right and left and are the relative momentum operators. The spin-exchange operator denoted by $\hat{P}_\sigma$ is:

$$\hat{p}_\sigma = \frac{1}{2}(1 + \hat{\sigma}_1.\hat{\sigma}_2) \quad \textbf{(5)}$$

A proper analysis of the surface characteristics, including the influence of the finite-range force, requires consideration of the momentum-dependent parameters [15]. Initially, a self-consistent shell model was used. For iterative computations, the Hartree-Fock mean field and the Skyrme interaction were used. For this purpose, the SLy4 force method was used [16]. Real WS and HO potentials, when added to this, provide a valid Skyrme force representation [13].

In electron scattering, nuclear form factors can be categorized as the longitudinal Coulomb form factor, $F(C\lambda, q, f, i)$, which describes inelastic transitions between initial (i) and final (f) nuclear states and reduces to elastic scattering when $i = f$. Additionally, the transverse form factors comprise the electric form factor, $F(E\lambda, q, f, i)$, and the magnetic form factor, $F(M\lambda, q, f, i)$, each associated with a specific multipolarity λ [17]. The transverse electric and magnetic form factors can be further decomposed into components arising from convection currents (λ_c) attributable to the orbital motion of nucleons and magnetization currents (λ_m) associated with the intrinsic magnetic moments of the nucleons [18].

$$F(E\lambda, q, f, i) = F(E\lambda c, q, f, i) + F(E\lambda m, q, f, i) \quad \textbf{(6)}$$

$$F(M\lambda, q, f, i) = F(M\lambda c, q, f, i) + F(M\lambda m, q, f, i) \quad \textbf{(7)}$$

The total longitudinal form factor is:

$$[F(C, q, f, i)]^2 = \sum_{\lambda \geq 0}[F(C\lambda, q, f, i)]^2 \quad \textbf{(8)}$$

and the total transverse form factor is:

$$[F(T, q, f, i)]^2 = \sum\{|F(E\lambda, q, f, i)|^2 + |F(M\lambda, q, f, i)|^2\} \quad \textbf{(9)}$$

Between the initial and final nuclear SM states with spin $J_{i,f,}$ the electron scattering form factor including angular momentum λ and momentum transfer q is given by [19]:

$$\left[F(X\lambda, q, f, i)\right]^2 = \frac{4\pi}{Z^2}\frac{1}{2J_i + 1}\left|\sum_{t_z}\left\langle n\omega_f J_f \left\| \hat{O}^\lambda(X, q, t_z) \right\| n\omega_i J_i \right\rangle\right|^2 F_{cm}^2 F_{fs}^2(q) \quad \textbf{(10)}$$

An X-designator selects the form factors for the *L* or *C* axis and the T axis. Each of the two form factors contains fundamental information about nuclear physics. For the different electron scattering operators, the elements of the single-particle matrix match those given in the works of Donnelly and Walecka [19] and Johnston and Drake [20]. The center-of-mass correction (F_{cm}) is the form factor used to describe a nucleon with a

finite size (F_{fs}), while $F_{fs}(q)$ is the adjustment designed to address the absence of translational invariance in the SM. The aggregate form factor is obtained by adding the longitudinal and transverse terms as:

$$|F(q)|^2 = |F_C(q,f,i)|^2 + [1/2 + tan^2(\theta/2)]|F_T(q,f,i)|^2 \quad \textbf{(11)}$$

θ denotes the angle of electron scattering.

Reduction in transition probability depends on the longitudinal (Coulomb) form factor at the photon point, which is described by [21]:

$$B(C\lambda) = \frac{Z^2e^2}{4\pi}\frac{[(2\lambda+1)!!]^2}{\omega^{2\lambda}}|F(C\lambda, q=\omega, f, i)|^2 \quad \textbf{(12)}$$

For magnetic transition [20]:

$$B(M\lambda) = \frac{Z^2}{4\pi}\frac{[(2\lambda+1)!!]^2}{\omega^{2\lambda}}\frac{\lambda}{\lambda+1}|F(M\lambda, \text{q=}\omega, \text{f, i})|^2 \quad \textbf{(13)}$$

B (*M1*) is in units of u_N^2, *B* (*C2*) is in units of e^2 fm^4, *B* (*M2*) is units of u_N^2fm^2, *B* (*C1*) is units of e^2 fm^2, where u_N is the nuclear magneton.

3. Results and Discussion

This study used the SM OXBASH [22] to compute the One-Body Density Matrix element (OBDM) components, which provide precise spectroscopic overlaps, eigenvectors, and energies for low-lying states in high-basis-dimensional shell model Hamiltonian matrix calculations. Using a *J*-coupled proton-neutron basis, the dimensions of the *J*-scheme matrices up to about 100 million were considered. The wrapper scripts convert the OXBASH output into tables and figures to show the energy levels, gamma decay, and beta decay. After that, the matrix elements of the coulomb Cλ, Eλ, and Mλ electric and magnetic multipole operators operations were computed using the OBDM components. In all our computations, the radial wave functions of the single-particle matrix components using a two-body Skyrme interaction potential were determined. This potential was derived from a one-body potential in Hartrre-Fock theory of types. The SM wave function with SHF potential was computed using the SLy4, parameterization, HO, and WS potentials in conjunction with the *spsdpf* model space with (0+1) ħω truncations [23]. To replicate the experimental data for transverse magnetic electron scattering of ^{12}C, ^{24}Mg, and ^{15}N, the oscillator size parameter b = 1.65 *fm* was employed. The valence model selected for all magnetic transitions was based on the data provided by Zarek et al. [7], Hicks et al. [8], and Salem [24].

3.1. ^{12}C (Negative Parity States)

The transverse electron scattering form factors corresponding to magnetic quadrupole (M2) transitions from the ground state to isoscalar excited states in the ^{12}C nucleus were evaluated for two low-lying states: the 2^-state at 12.180 MeV ($T = 0$) and the 2^-state at 16.660 MeV ($T = 1$). Fig. 1 presents the calculated transverse form factors based on shell model predictions using various single-particle potentials, over a momentum transfer range of $q = 0$–3 fm^{-1}.

In Fig. 1a, for the $2^-(T = 0)$ state at 12.180 MeV, the form factor computed with the Skyrme SLy4 potential exhibits strong agreement with experimental data, particularly at higher momentum transfers. The HO potential yields moderately

consistent results, while the WS potential fails to reproduce the experimental trend in the range $q = 1.3$–2.5 fm^{-1}. The smoother decline and simpler shape of the form factor may reflect the underlying symmetry in proton-neutron distributions for this isoscalar transition.

In contrast, Fig. 1b illustrates the $2^{-}(T = 1)$ state at 16.660 MeV, for which none of the models fully reproduce the experimental data. While the HO potential captures the approximate position of the form factor peak, it fails to replicate the overall shape. The WS potential shows slightly better agreement in some regions, but remains inadequate overall. The SLy4 potential provides a comparatively better match at high momentum transfers, consistent with the expected behavior for isovector ($\Delta T = 1$) transitions. The form factor profiles for the $T = 1$state exhibit more pronounced fluctuations, likely indicative of the asymmetric proton-neutron configurations in the excited state. Notably, as the momentum transfer increases, the form factors for both isoscalar and isovector transitions show a trend toward qualitative convergence.

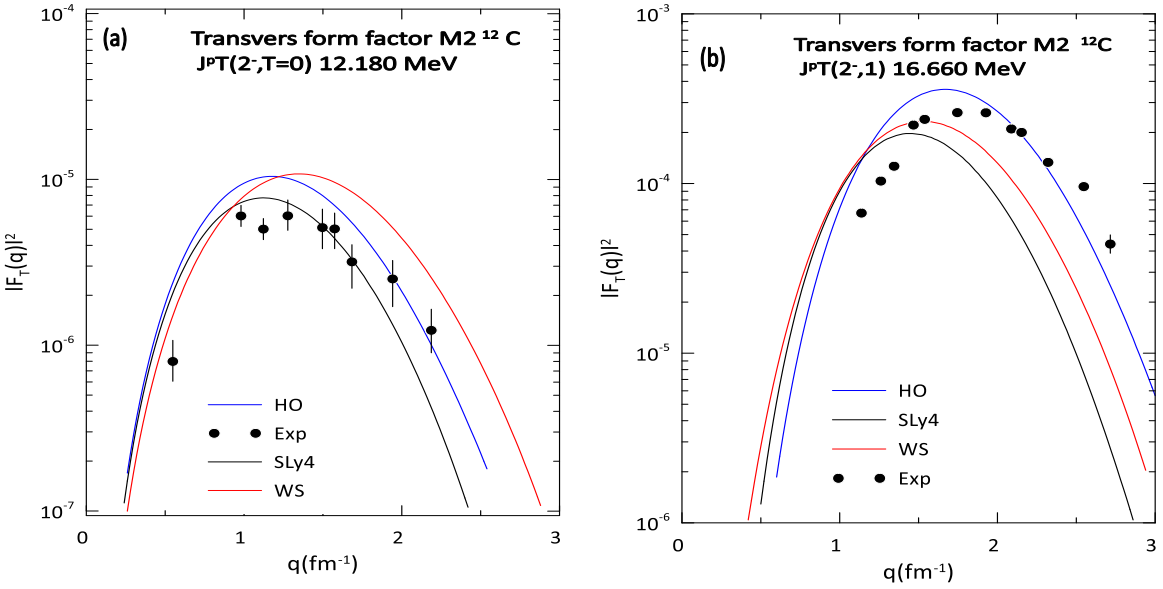

Figure 1: Transverse form factor (2⁻,0) and (2⁻,1) at (12.180, 16.660) MeV states with various single potential compared to experiment results [8].

3.2. ^{24}Mg (Negative Parity states)

Fig. 2 shows the transverse form factors for a specific nuclear state 2^{-} at 12.666 MeV using various single-particle potentials compared to experimental data [7]. This comparison evaluates how the theoretical models based on these potentials match the experimental data. In this case, the HO potential yields a closer fit to experimental findings for the transverse form factor of the 12.666 MeV states since it is in better agreement with the experimental data. This suggests that HO may be more suitable or accurate for describing scattering processes at this energy level.

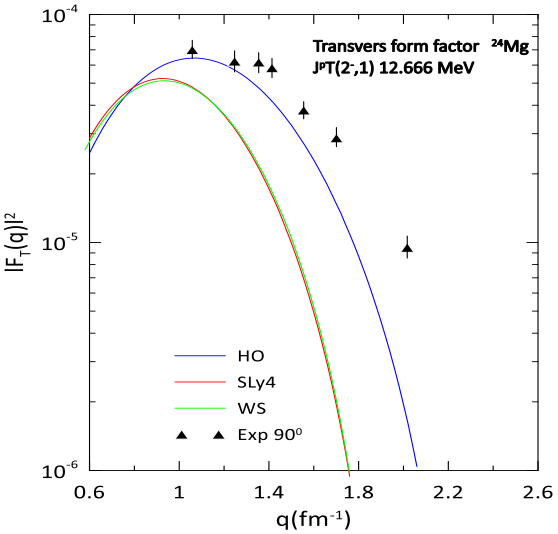

Figure 2: Transverse form factor (2⁻,1), 12.666 MeV state with Θ=90⁰ compared to the results of experiments utilizing various single particle potentials [7].

3.3. ^{15}N (Positive Parity States)

Fig. 3 presents the calculated transverse electron scattering form factors in comparison with experimental data for the $3/2_3^+$ and $3/2_4^+$ states at 10.062 MeV and 10.800 MeV, respectively. The experimental values were recalculated for the maximum incident electron energy, employing different single-particle potentials. As shown in Fig. 3a, the calculated transverse form factor for the $3/2_3^+$ state tends to overestimate the experimental data; however, it follows the general trend reasonably well. Notably, a point of correspondence between theory and experiment is observed at $q = 1.75$ fm^{-1}. Fig. 3b displays the transverse magnetic quadrupole M2 form factor for the $3/2_4^+$ state, calculated using both the HO and WS potentials. The theoretical profiles exhibit good agreement with the experimental data in the low momentum transfer region. Furthermore, the first peak of the form factor is well reproduced, although the theoretical prediction fails to accurately replicate the position of the second peak. To improve the agreement between theory and experiment, effective charges based on the formalism of Bohr and Mottelson [25] were employed, with δ_p =0.1453 and δ_n =0.7453.

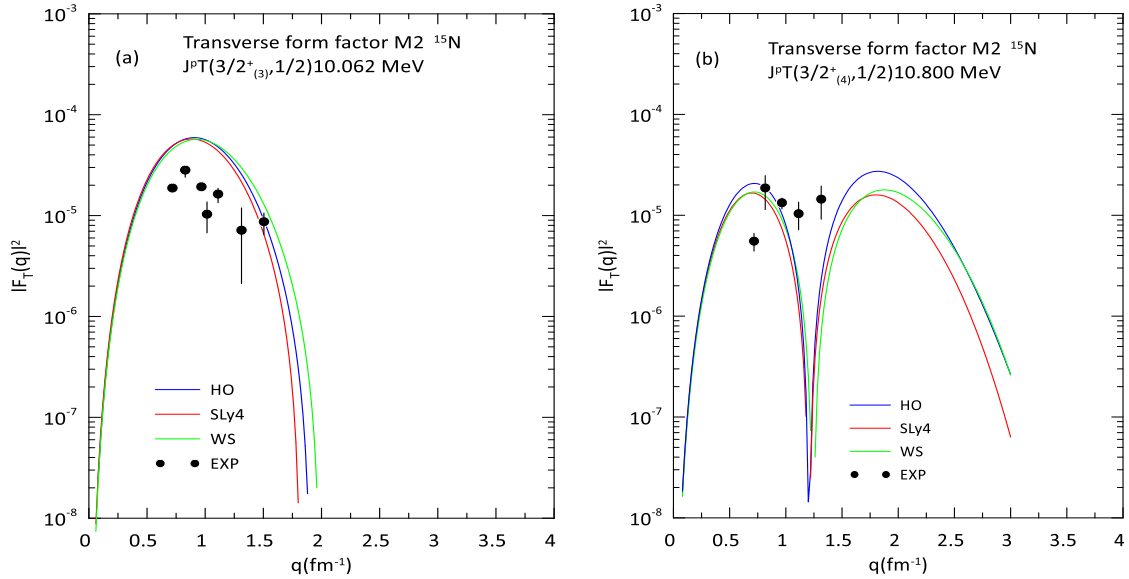

Figure 3: Transvers form factor (a) 3/2⁺(3) state 10.062 MeV (b) 3/2⁺(4) state 10.800 MeV compared with the results of experiments utilizing various single particle

Fig. 4a illustrates the theoretically calculated transverse M2 form factor for the purely magnetic $5/2_2^+$transition, obtained using various single-particle potentials. The theoretical predictions exhibit poor agreement with the experimental data, failing to accurately reproduce the observed form factor shape. Despite attempts to refine the calculations, no significant improvement was achieved. The predicted M2 form factors for this transition are confined to a low momentum transfer region, suggesting a need to adjust the parameters of the employed single-particle potentials.

Fig. 4b presents the calculated transverse M2 form factor for the $5/2_4^+$state. The form factor calculated using the HO potential shows good overall agreement with experimental data across the entire momentum transfer range. Moreover, the form factor profile appears relatively insensitive to changes in the choice of single-particle potential; however, a gradual divergence from experimental data is observed as the momentum transfer increases. Notably, at the peak location, the experimental value is lower than the SM prediction. These calculations were performed using effective charges.

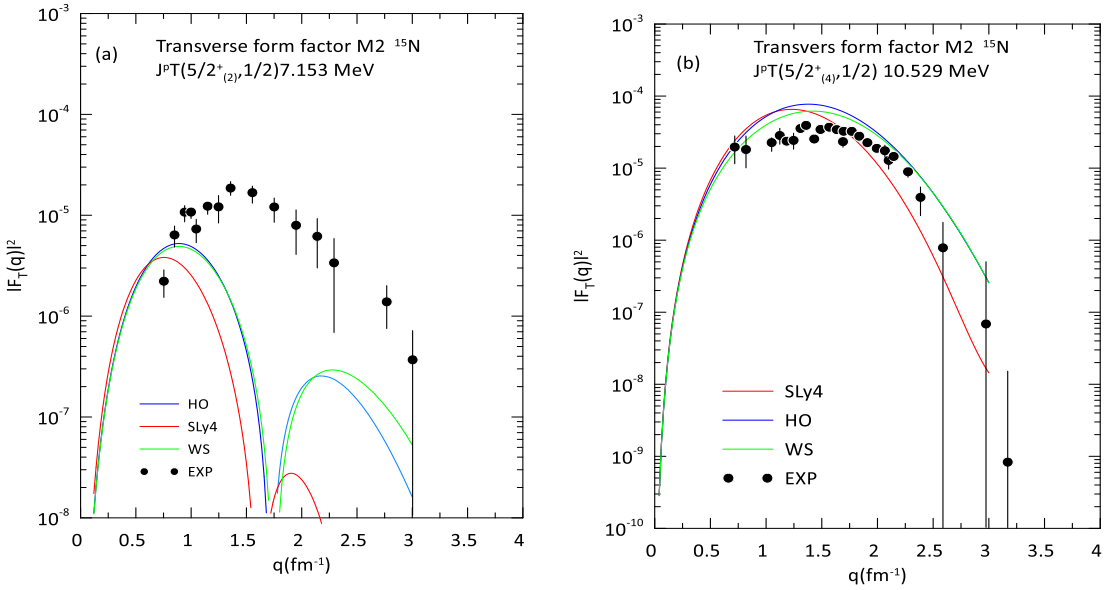

Figure 4: Transvers form factor (a) 5/2$^+_{(2)}$ state 7.153 MeV (b) 5/2$^+_{(4)}$ state 10.529 MeV compared with the results of experiments utilizing various single particle potentials [24].

4. Conclusions

We are currently conducting further research on the application of the SHF with SM findings to investigate the nuclear structure of ^{12}C, ^{15}N, and ^{24}Mg nuclei with changing parity states. This study considered three single-particle potentials, namely the Skyrmee SLy4, HO, and WS potentials, for the inelastic electro-excitation form factors within the momentum-transfer range of $0.0 < q < 3.0$ fm^{-1}. Among all the potentials employed, the HO potential exhibited the most accurate reproducibility of the experimental results. Our computations indicated that the replicated form factors can be determined using the *spsdpf* SM spaces with WBP effective interaction. The calculated transverse form factors for the ^{12}C nucleus show closer agreement with experimental data for the $T = 0$ states compared to the $T = 1$ states. This improved agreement is attributed to the more accurate parameterization applicable to isoscalar transitions, whereas the $T = 1$states likely involve more complex nuclear interactions that are not as well constrained. The differing behavior observed in the $2^-, 1$ form factors between ^{12}C and ^{24}Mg can be

primarily attributed to differences in their underlying nuclear structure and nucleon distribution. ^{12}C form factor is influenced by its simpler and more symmetric nuclear configuration, while ^{24}Mg exhibits more complexity due to its larger number of nucleons and potential nuclear deformation effects. The experimental values were smaller than the SM predications in ^{15}N nucleus. In contrast to previous expected transverse form factors, the predicted transverse form factors for these transitions in the $5/2^{+}_{(2)}$ state exhibited the opposite behavior. The effective charge of this transition was calculated to improve the results.

Acknowledgments

The authors express gratitude to the University of Baghdad, College of Science, Department of Physics, for their assistance with this paper.

Conflict of Interest

The authors declare that they have no conflict of interest.

References

1. M. Bender, P.-H. Heenen and P.G. Reinhard, Rev. Mod. Phys. **75**, 121 (2003) https://doi.org/10.1103/RevModPhys.75.121.
2. P. Sarriguren, D. Merino, O. Moreno, E. Moyade Guerra, D. N. Kadrev, A. N. Antonov, and M. K. Gaidarov, Phys. Rev. C **99**, 034325 (2019). https://doi.org/10.1103/PhysRevC.99.034325.
3. B.A.Brown, Prog. Part. Nucl. Phys, **47**, 517 (2001). https://doi.org/10.1016/S0146-6410(01)00159-4.
4. B. A. Brown and B. H. Wildenthal, Annu. Rev. Nucl. Part. Sci. **38**, 29 (1988) https://doi.org/10.1146/annurev.ns.38.120188.000333.
5. Y. Kanada-En'yo and K. Ogata, Phys. Rev. C**103**, 024603 (2021). https://doi.org/10.1103/PhysRevC.103.024603.
6. N. S. Manie and A. A. Alzubadi, Iraqi J. Phys. **17**, 42 (2019). https://doi.org/10.30723/ijp.v17i42.421
7. H. Zarek, S. Yen, B.0. Pich, T. E. Drake, C. F. Williamson, S. Kowalski, and C. P. Sargent, Phys.Rev., C **29**, 1664 (1984). https://doi.org/10.1103/PhysRevC.29.1664.
8. R. S. Hicks, J.B.Flanz, R. A. Lindgren, G. A. Peterson, L. W. Fagg and D. J. Millener, Nucl. Phys. C**30**, 1(1984). https://doi.org/10.1103/PhysRevC.30.1
9. A. A. Alzubadi and Luma J. Abbas, Phys. At. Nucl. **86**, 370 (2023). https://doi.org/10.1134/S1063778823040026
10. A. A. Alzubadi,, Iraqi J. Phys. **14**, 28 (2016). https://doi.org/10.30723/ijp.v14i31.169.
11. A.A. AL-Sammarraie, F.A. Ahmed, A.A. Okhunov, Ukr. J. Phys. **66**, 295 (2021) https://doi.org/10.15407/ujpe66.4.293.
12. P. Sarriguren, O. Moreno, E. Moya de Guerra, D.N. Kadrev, A.N. Antonov, and M.K. Gaidarov, *J. Phys.: Conf. Ser.,* **1555**0, 12001 (2020) https://doi.org/10.1088/1742-6596/1555/1/012001.
13. A. A. Alzubadi, R. A. Radhi, and N. S. Manie, Phys. Rev. C **97**, 024316 (2018). https://doi.org/10.1103/PhysRevC.97.024316.
14. G. W. Harby and A. A. Alzubadi Iraqi J. Phys. **20**, 40 (2022). https://doi.org/10.30723/ijp.v20i3.1004.
15. H. Sagawa, B. A. Brown, and O. Scholten, Phys. Lett. B, **159**, 228 (1985). https://doi.org/10.1016/0370-2693(85)90240-0.
16. E. Chabanat, R. Bonche, R. Haensel, J. Meyer, R. Schaeffer, Nucl. Phys. A, **635**, 231 (1998). https://doi.org/10.1016/S0375-9474(98)00180-8.
17. T. de Forest and J. D. Walecka, Adv. Phys., **15**, 1 (1966). https://doi.org/10.1080/00018736600101254.
18. B. A. Brown, B.H. Wildenthal, C. F. Williamson, F.N. Racl, S. Kowalski, and J. T. O'Brien, Phys. Rev., C **32**, 1127 (1985). https://doi.org/10.1103/PhysRevC.32.1127.
19. T. Donnelly and J. D. Walecka, Ann. Rev. Nucl. Sci. **25**, 329 (1975). https://doi.org/10.1146/annurev.ns.25.120175.001553.
20. A. Johnston, T. E. Drake, J.Phys. A:Math. Gen.**7**, 8 (1974).https://doi.org/ 10.1088/0305-4470/7/8/004.
21. R. A. Radhi, Ph.D. Thesis Michigan State University, (1983).
22. B. A. Brown, Msu-Nscl- Repo. 1289 (2004).
23. B. A. Brown, R. A. Radhi, and B. H. Wildenthal, Phys. Rep., **101**, 313 (1983). https://doi.org/10.1016/0370-1573(83)90001-7.

24. S. A. Salem, Ph.D. Thesis, University of Glasgo, (1987).
25. A. Bohr and B. R. Mottelson, *Nuclear Structure*, Vol. 2 (Benjamin, New York, 1975).

التشتت الإلكتروني غير المرن (M2) لتغيير حالات التكافؤ لـ ^{12}C و^{15}N و^{24}Mg

علي خالد عبود[1] و علي عبداللطيف كريم[1]
[1] قسم الفيزياء، كلية العلوم، جامعة بغداد، بغداد، العراق

الخلاصة
تتناول هذه الدراسة البنية النووية لنوى الكربون-12 والنيتروجين-15 والمغنيسيوم-24 باستخدام نموذج القشرة (SM) مع منهج سكايرم هارتري-فوك (SHF). وقد حُسبت عوامل الشكل لتشتت الإلكترونات غير المرن للحالات ذات الطاقة المنخفضة التي تغير تكافؤها. وتُظهر هذه الدراسة جدوى هذه الاستراتيجية باستخدام فضاء نموذج القشرة spsdpf واسع النطاق المقتطع مع تفاعل WBP الفعال ثنائي الجسم. تشير بيانات حالات الانتقال M2 (2-,0) و(2-,1) إلى مستويات طاقة تبلغ 12.180 ميغا إلكترون فولت و16.660 ميغا إلكترون فولت في الكربون-12، و12.666 ميغا إلكترون فولت في المغنيسيوم-24، و10.062 ميغا إلكترون فولت و10.800 ميغا إلكترون فولت للحالتين 2/3+(3) و2/3+(4)، و7.153 ميغا إلكترون فولت و10.529 ميغا إلكترون فولت للحالتين 2/5+(2) و2/5+(4) في النيتروجين-15. في إطار نظرية هارتري-فوك، تُستخدم تفاعلات سكيرم لاستنتاج جهد أحادي الجسم لحساب عناصر المصفوفة للجسيم الواحد. ويُظهر جهد الجسيم الواحد للمذبذب التوافقي (HO) وجهود وودز-ساكسون (WS) وجهود هارتري-فوك المفردة (SHF) لعوامل الشكل غير المرنة توافقًا ملحوظًا مع البيانات التجريبية المتوفرة.

الكلمات المفتاحيه: نموذج شل، سكايرم هارتري-فوك، تغيير حالة التكافؤ، التشتت الإلكتروني غير المرن، عامل الشكل العرضي.